Alexandria Engineering Journal (2022) 61, 8943–8953

HOSTED BY

Alexandria University

Alexandria Engineering Journal

www.elsevier.com/locate/aej
www.sciencedirect.com

Thermal performance enhancement of nanofluids based parabolic trough solar collector (NPTSC) for sustainable environment

M. Farooq [a,b,*], M. Farhan [a,b], Gulzar Ahmad [c], Zia ul Rehman Tahir [a], M. Usman [a], M. Sultan [d], M. Saad Hanif [b], M. Imran [c,*], Saqib Anwar [e], Ahmed M. El-Sherbeeny [e], M. Ali Shakir [f]

[a] Department of Mechanical Engineering, University of Engineering & Technology (UET), Lahore 54800, Pakistan
[b] Center for Energy Research & Development (CERAD), University of Engineering & Technology (UET), Lahore 54800, Pakistan
[c] Department of Mechanical, Biomedical and Design Engineering, Aston University, B4 7ET, Birmingham, UK
[d] Department of Agricultural Engineering, Bahauddin Zakariya University, Bosan Road, Multan 60800, Pakistan
[e] Industrial Engineering Department, College of Engineering, King Saud University, P.O. Box 800, Riyadh 11421, Saudi Arabia
[f] Department of Mechanical Engineering, College of Engineering and Technology, University of Sargodha, Sargodha 40100, Pakistan

Received 1 October 2021; revised 20 January 2022; accepted 12 February 2022
Available online 25 February 2022

KEYWORDS

PTSC;
Nanofluids;
Thermal efficiency;
Solar thermal;
Temperature difference

Abstract Due to rapid industrialization and urbanization, upward rise in carbon emissions in the atmosphere, and depletion of fossil fuel and gas reserves have forced to find alternative renewable energy resources, where solar energy is one of the most promising source. Parabolic trough solar collectors (PTCs) can effectively transfer high temperature in the tube of receiver upto 400 °C. In this study, Computational Fluid Dynamics (CFD) analysis is used to analyse the effect of multiple working fluids on efficiency of the PTC. Two different types of nanofluids used for analysing the thermal efficiency of PTC through CFD simulations, are Alumina and Copper-oxide nanofluids. The concentration of Copper Oxide and Alumina was kept to 0.01% in the nanofluids. The efficiency for PTC is calculated at two different mass flow rates i.e., 0.0112 Kg/s and 0.0224 Kg/s. The highest efficiency is 13.01 and 13.1% using Al_2O_3 as nanofluids at 0.0112 Kg/s and 0.0224 Kg/s flow rates, while CuO has an efficiency of 13.92% and 14.79% for these flow rates. The behaviour of absorber tube material on temperature distribution for steel, copper and aluminum as absorber tube material was also investigated. Changing the material from steel to copper and aluminum increased the outlet temperature of the fluid. The maximum output temperature was achieved for copper is 311 K while steel and aluminum showed lower temperature of 307 K and 308 K of the fluid at the outlet. Furthermore, the impact of the receiver tube's length on the working

* Corresponding authors.
E-mail addresses: engr.farooq@uet.edu.pk (M. Farooq), m.farhan@uet.edu.pk (M. Farhan), gulzar_uetian@hotmail.com (G. Ahmad), ziartahir@uet.edu.pk (Z.R. Tahir), muhammadusman@uet.edu.pk (M. Usman), muhammadsultan@bzu.edu.pk (M. Sultan), saadbinhanif31@gmail.com (M. Saad Hanif), m.imran12@aston.ac.uk (M. Imran), sanwar@ksu.edu.sa (S. Anwar), aelsherbeeny@ksu.edu.sa (A.M. El-Sherbeeny), ali.shakir@uos.edu.pk (M. Ali Shakir).

Peer review under responsibility of Faculty of Engineering, Alexandria University.

https://doi.org/10.1016/j.aej.2022.02.029

Nomenclature

Nu	Nusselt's number	μ	Dynamic viscosity
Δ	Gradient	Pr	Prandtl number
Cp	Specific heat of gas at constant pressure	W	Width of NPTSC
η_{th}	Thermal efficiency	G_{av}	Average value of solar radiation
η_o	Overall efficiency	S	Absorbed Heat flux
G_T	Solar intensity	K	Thermal conductivity
¥	Specular reflectivity	v_r	Radial direction of velocity
Rb	Bond resistance	v_x	Axial direction of velocity
α	Absorptivity of receiver tube	μ	Fluid viscosity (in Kg/m-s)
τ	Glass envelope transmissivity	Ave	Average
A_{ap}	Aperture area		

fluid's temperature is also studied. Copper Oxide nanofluid has higher temperature at the outlet for both mass flow rates as compared to alumina nanofluid. Accordingly, a comparison was made for the CFD results with the experimental findings from literature. The nanofluids based PTCs system is promising method for the sustainable environment applications.

1. Introduction

The increasing demand of energy and available resources is becoming a huge challenge today, where, solar energy, one of the promising and great source of renewable energy [1]. The surface of the earth is recorded to intercept an average of 3.6 × 1014 TW of solar radiations [2,3]. Solar thermal collectors are among the most popular source of renewable energy [4]. PTSC uses direct solar radiations for heating the working fluid [5]. A glass envelope is used to enhance the collector performance and to minimize the losses of convection [6]. The sunlight intensity is increased by using this configuration and the heat generated by sunlight on the receiver. Temperature range for operation of working fluid in PTCs is between 50 °C and 400 °C. About 30% of the PTC system's cost is accounted by solar receiver [17]. A solar tracking system is usually used for efficiency enhancement by changing the position in the direction of sun. Parabolic troughs can be arranged in various sizes in the solar fields and can be linked together easily. However, the axis of the collector must be oriented in North-South or East-West direction to minimize the losses. Therefore, single-axis tracking is mostly used for achieving this purpose. PTSC provides advantage of higher efficiency with low surface area requirement even with diffused sun light for same output. PTSC can be used on roof surfaces orienting on non-south direction [7,8]. Higher temperatures can be produced with PTSC and also provides advantage of integrating with high-temperature systems. The concentrators are made of recyclable materials which reduce the environmental waste as well [9].

The trackers concentrate the sunlight effectively and transfer converted heat to a working fluid. This phenomenon is steady-state, and working fluid in the annular region with high specific heat is preferred [10]. Conventional Newtonian working fluids constitute water, molten salt, and air flowing through the collectors. These fluids have poor thermophysical properties, hence, lower the efficiency of the collectors [11]. The main parameter in increasing PTSC efficiency is geometry modeling, working fluid selection and receiver tube material [12]. Molten salts were used a working fluids yielding excellent thermal conductivity, reduced corrosion and clogging in the components of the receiver tube. The rate of absorptivity is also very high in the UV-visible region. Furthermore, size and other properties can also be finetuned at atomic level bottom up to achieve a much higher conductive phase [13]. The applications of nanofluids have increased with increase in their popularity, and use in medical devices, solar energy, fuel cells and heat exchangers have been explored [14]. Nanofluids have a great potential in PTSCs as it can help significantly reduction in the cost of the system [15–17]. Selective coatings of black-chrome or black nickel is used for non-evacuated receivers because of their economic reasons and ease of production [18]. The maximum length of the receiver tube is 5 m because of manufacturing constraints, therefore, the tubes are connected in series to obtain the desired length of PTC [19]. The performance of PTSCs is affected by the geometric parameters and the materials [20]. Semi-finite analytical formulation was reported in the literature, which depicts that the semi-finite method requires special integration, geometrical and optical characteristics are not changed easily by using this method [21]. These methods are used for determining the efficiency, heat flux and absorber tube material in various researches [22–24]. In another study, enhancement upto 4.3% in the PTC performance system using oil/Al_2O_3 nanofluid [25,26]. The usage of hybrid nanofluids with dual characteristics is receiving recognition over the last few years. Hybrid nanofluid is synthetized by splitting two nanoparticles (NP) types within the host fluid. Using this technology in solar collector applications is scarce due to many problems in expressing the thermophysical characteristics of hybrid nanofluids [27].

Computational fluid dynamics (CFD) analysis of (Al_2O_3 and CuO) NP was carried out in solar collectors, where, the heat transfer coefficient reached 28%-35% when dispersed in water [29,30]. Nanofluids more efficiently capture the solar radiation, hence, nanofluids are considered as an efficient for PTCs. The concentration of nano particles within the fluid and diameter of the nano particles are some of the significant parameters for the effiencent system [31]. Using CFD analysis, it was found that Oil/ Al_2O_3 nanofluid increases the performance of NPTSC to 4.25% [32,33]. Another study demonstrates that the CuO is an efficient NP, resulting in a 1.3% increase in thermal performance while the Al_2O_3 NP is 1.12%, however, 40% decrease in the pressure was also observed by using such system [34]. In another study, it was found that the maximum heat transfer is achieved at 2% Al_2O_3 concentration. So, it is concluded that Al_2O_3 nanofluid is the best thermal-physically while the CuO is the best exegetically. The usage of hybrid nanofluids with dual characteristics is receiving recognition over the last few years [35–37]. Hybrid nanofluid is synthetized by splitting two NP types within the host fluid. Using this technology in solar collector applications is scarce due to many problems in expressing the thermophysical characteristics of hybrid nanofluids [38]. The thermal efficiency of PTSC is improved by taking copper as compared to steel and aluminum. The temperature distribution in case of copper also remains the same throughout the length of the tube [39]. However, for steel a parabolic shaped temperature distribution is achieved. In addition, the aluminum and galvanised steel have poor corrosivity as compared to coper and stainless steel [40]. Therefore, aluminum and galvanized steel are not used for construction of absorber tube despite of their low prices [41]. The receiver tube made of copper was termed as most suitable because of its moderate cost and low corrosion resistance. On the other hand the corrosion resistance of stainless steel was high as compared to copper, however, the cost of stainless steel was also high as compared to copper. The gap between the absorber and reflective tube must be kept optimum for decreasing the convection heat losses [42]. The convective heat losses decreases as the internal diameter is increased until the optimum distance was achieved [43]. Creating vacuum at this distance increases the performance of the system and the gap length governs the heat losses occurring within the system. This distance is known as critical radius and depends upon the diameter of the glass envelope used [44]. Smaller size diameter NP increased heat transfer rate in PTSC. It was reported that the concentration and flowrate of NP are used to enhance the thermophysical characteristics of the working fluid in PTSC [45,46]. Borosilicate is considered as the choice of material for glass tube as it has high tolerance against thermal shocks [47]. The selective coating absorbs the solar energy and conduct the energyinside the tube [48]. There is a shortage of data of hybrid nanofluids performance in concentrating PSCs [49].

In this study, CFD simulations are used to analyse the behavior of different nanofluids on thermal performance in NPTSC. The model is meshed using ANSYS Fluent and validated with the help of experiments from the studies reported in the literature. Then validated model was applied to different flow conditions of nanofluids and material properties to perform a parametric study. Thermal performance of NPTSC is also affected by the change in material of the absorber tube. Depending on the thermal conductivity of the tube material, thermal efficiencies were calculated and analysed in details.

2. Methodology

CFD simulations were used to analyse the behaviour of absorber tube material and effect of flow rate on efficiency. The simulation was carried out using two different tye of nanofluids (Al_2O_3 and CuO) with two values of 0.0112 Kg/s and 0.0224 Kg/s. The volume concentration of both nanofluids was kept constant at 0.01% [27]. Three different materials used for calculating performance are steel, aluminum, and copper and different characteristics are given in the Table 1. The simulations were performed at steady-state conditions with a radiation model in ANSYS FLUENT.

Temperature contours for each mass flow rate were also obtained. The optical errors of the reflector were neglected. The nanofluid was considered incompressible and turbulent, and the vacuum was considered an annular space to minimize the losses. The configuration used in the study is shown in Fig. 1.

2.1. Geometry modeling

The receiving tube is modeled using Ansys. The geometry consists of concentric tubes (glass envelope and receiver) with fluid regions for the nanofluid and the (annular region) with vacuum, respectively. Geometry was oriented along the z-axis, where, the positive Z and X-axis denotes the south and east directions, respectively. Following specifications are related to geometry:

a) The concentrating reflector is parabolic, used for concentrating solar radiation, and is made of aluminum. Parabolic mirrors reflect the sunlight parallel to its focal line with 96% efficiency [27].

b) The receiver tube is made up of a 1.22 m Copper tube coaxed within a glass envelope; with a maintained flow rate of nanofluids. The outer diameter and inner diameter of the absorber tube are 27 mm and 28 mm, respectively, to give a good concentration ratio of about 10 depending on the trough

Table 1 Material Specifications [50–52].

Selected Materials	Density of the Materials (Kg/m^3)	Thermal Conductivity (W/m-K)	Specific Heat Capacity (KJ/Kg)	Corrosion Rate (μm/year)	Receiver Tube Cost ($)
Steel	8030	16.27	502.48	0.21	149.38
Aluminum	2719	202.4	871	3.7	23.55
Copper	8978	381	387.6	1.27	33.38
Glass	2200	1.75	9.1		

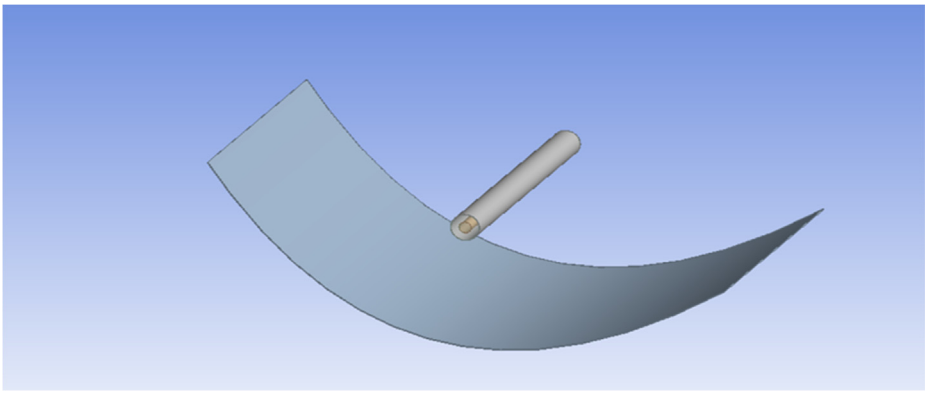

Fig. 1 Configuration of the Solar Collector.

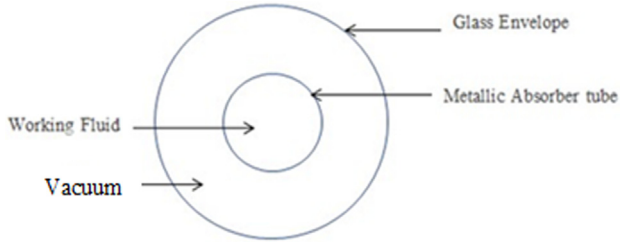

Fig. 2 X-Sectional representation of the Solar Collector Tube.

size. The tube was placed parallel to the focal length. The absorber tube was painted black so that maximum solar irradiations are absorbed by the tube. Heat losses are minimized. Glass envelope tube with 0.91 m length of 64 mm and 66 mm inner and outer diameter, respectively. The geometry for the tube of the collector is given in Fig. 2.

2.2. Meshing of the receiver tube

Fig. 3 shows the mesh for the collector tube and solar trough collector. Ansys Fluent was used for mesh generation of modelled tube. The quality of mesh plays an important role in obtaining accurate results. Initially, Hexahedral cells were created that composed of 259,435 elements and the difference in temperature is measured and described in Table 2. There was a negligible difference between the results obtained from 520,141 and 672,400 grid sizes. Therefore, 520,141 cells were chosen s for further studies to save computational time and cost.

2.3. Thermo-physical properties of materials

Table 3 shows various thermo-physical properties of fluid and glass.

2.4. Physical modelling

Flow behaviour model, energy model, solar load model, and radiation model were employed to carry out the numerical simulations. In flow behavior model, CFD analysis were performed for the receiver tube and to study heat convection flow of nanofluid. The energy model demonstrates an energy balance between the nanofluid and the receiver tube. The model assumes that all thermodynamic properties of nanofluid are constant and the model is computed using Engineering Equation Solver (EES) [28]. The solar load model was used for computing various inputs of location, analysis day timings, and mesh orientation. Total radiation (sum of the beam and diffuse radiation) was used in simulation. The radiation model is used for modelling radiation heat transfer. Heat loss and transfer simulation were modelled using the Surface-to-Surface (S2S) model to consider various factors,

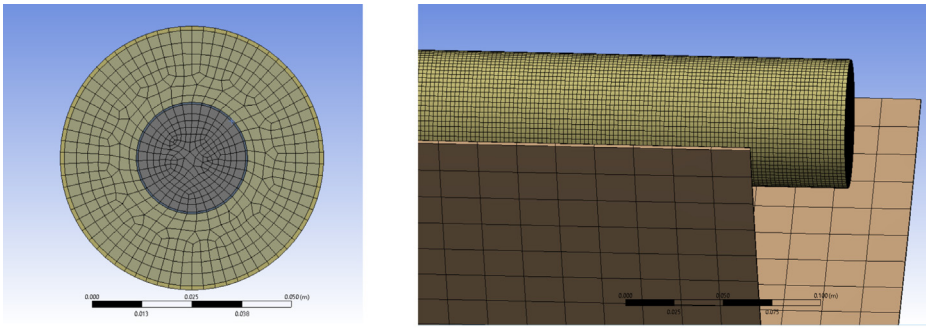

Fig. 3 Mesh for (a) Collector tube, (b) Solar Trough Collector.

Table 2 Grid Sensitivity test.

Mesh Size	Number of Element	The Difference between inlet and outlet temperatures (°C)
Very Coarse	259,435	5.05
Coarse	406,586	4.36
Medium	520,141	4.21
Fine	672,400	4.13
Very Fine	734,184	4.15

including radiation exchange from glass envelope to the receiver tube.

2.5. Governing equations

The number of equations were used for the CFD analysis including active transport expression, conservation of energy, Initial density of nanofluid relation, thermal efficiency and overall efficiency [53].

a) Continuity equation is given

$$\frac{\partial\left(\rho\, u_i\right)}{\partial x_i} = 0 \tag{1}$$

$$\frac{\partial\left(\rho\, u_i\, u_j\right)}{\partial x_i} = -\frac{\partial p}{\partial x_i} + \frac{\partial}{\partial x_j}\left[\mu\left(\frac{\partial u_i}{\partial x_j} + \frac{\partial y}{\partial x_i} - \frac{2}{3}\delta_{ij}\frac{\partial u_i}{\partial u_j}\right)\right] \tag{2}$$

b) Momentum equation

$$\rho\frac{Du}{Dt} = \frac{\partial(\rho u)}{\partial t} + \nabla.(\rho u V^{\leftarrow}) \tag{3}$$

c) Active transport expression

$$\left(\frac{\partial y}{\partial x}\right)(u_i u_j) \tag{4}$$

d) Energy conservation equation

$$\rho\frac{De}{Dt} = \frac{\partial(\rho e)}{\partial t} + \nabla.(\rho e V^{\leftarrow} \tag{5}$$

$$\frac{\partial(\rho\, u_j T)}{\partial x_j} = \frac{\partial}{\partial x_j}\left[\frac{\lambda}{C_p}\frac{\partial T}{\partial x_j} - \delta u_j' T'\right] + S_h \tag{6}$$

Table 3 Thermo-Phyiscal Properties of Fluid Materials [13,17].

Properties	Waterwith Al_2O_3 (0.01% conc.)	Water with CuO (0.01% conc.)	Glass
Density (Kg/cm^3)	1029.7	1054	2200
Specific heat (KJ/Kg-K)	4.05507	3.965	910
Thermal Conductivity (W/mK)	1.029	0.6870	1.75
Viscosity (m^2/s)	0.405×10^{-6}	0.396×10^{-6}	–
Dynamic Viscosity (m^2/s)	4.169×10^{-4}	4.169×10^{-4}	–

e) Initial density of nanofluid is ρ_0 is given by

$$\rho = \rho_o(1 - \beta\Delta T) \tag{7}$$

Change in the value of density is considered negligible and $\beta(T - T_0) \ll 1$. Simulated results can be obtained with more accuracy when density is taken as a function of temperature.

Following relations are used to calculate the different efficiencies including instantaneous and thermal efficiency [53].

Absorbed Heat flux

$$S = G_T R_b(\alpha\tau)¥Y \tag{8}$$

Convective heat transfer is dependent on Nusselt's number (Nu)

$$h_f = N_u.\frac{k}{D_i} \tag{9}$$

Where, Nu = Re0.8Pr0.4, $Pr = \frac{\mu C_p}{K}$,

$$Re = \frac{\rho V Di}{\mu}$$

$$V = \frac{4\dot{m}}{\pi D_i^2 \delta}$$

Thermal efficiency [53]:

$$\eta_{th} = \frac{\dot{m}c_p(T_{out} - T_{in})}{A_{ap}G_T t} \tag{10}$$

Overall efficiency:

$$\eta_o = \frac{\dot{m}c_p(T_{out} - T_{in})}{A_{ap}G_{av}} \tag{11}$$

2.6. Boundary conditions

Different boundary conditions were applied to solve differential equations. A range of mass flow rate with an increment of 0.0112 Kg/s was provided at inlet of the tube and initial temperature of working fluid was set as 302 K. Pressure boundary conditions was applied at the outlet of the tube. The operating pressure was kept constant to 101,325 Pa. Monitors were created for variables of interest before simulating the model. Convergence criteria was predefined and the normalized absolute residuals for all the variables in each cell have been limited to be less than 10^{-4}. For glass envelope only radiative mode for considered for heat losses. The average values of absorptivity and emissivity of black paint are taken as 0.95 and 0.91 respectively.

2.7. Model validation

A comparison of the CFD results is necessary to validate the performance of NPTSC with the experiments reported in the literature. Flow behaviour model, energy model, solar model, and radiation model were employed in ANSYS for simulations and the results are compared with experimental data. At the same time, parameters such as the geometry of the receiver tube and thermophysical properties of nanofluids were kept the same to match the experimental readings. The Table 4 compares the experimental data from the study reported in the literature [27] and simulated data for water, Al_2O_3, and CuO. Comparison agrees with the behaviour of different

Table 4 Comparison of different parameters of simulations with experiments at flow rate of 0.112 Kg/s.

Working Fluid	DNI (W/m^2)	Inlet Temperature (K)	Experimental [27]		Numerical		ΔT%
			Outlet Temperature (K)	Thermal Efficiency (%)	Outlet Temperature (K)	Thermal Efficiency (%)	
Water	788	305	309.25	12.06	309.32	12.137	0.6
0.01% Al_2O_3	788	305.55	309.65	12.46	309.70	12.62	1.2
0.01 % CuO	788	306.25	311.25	13.56	311.31	13.68	0.8

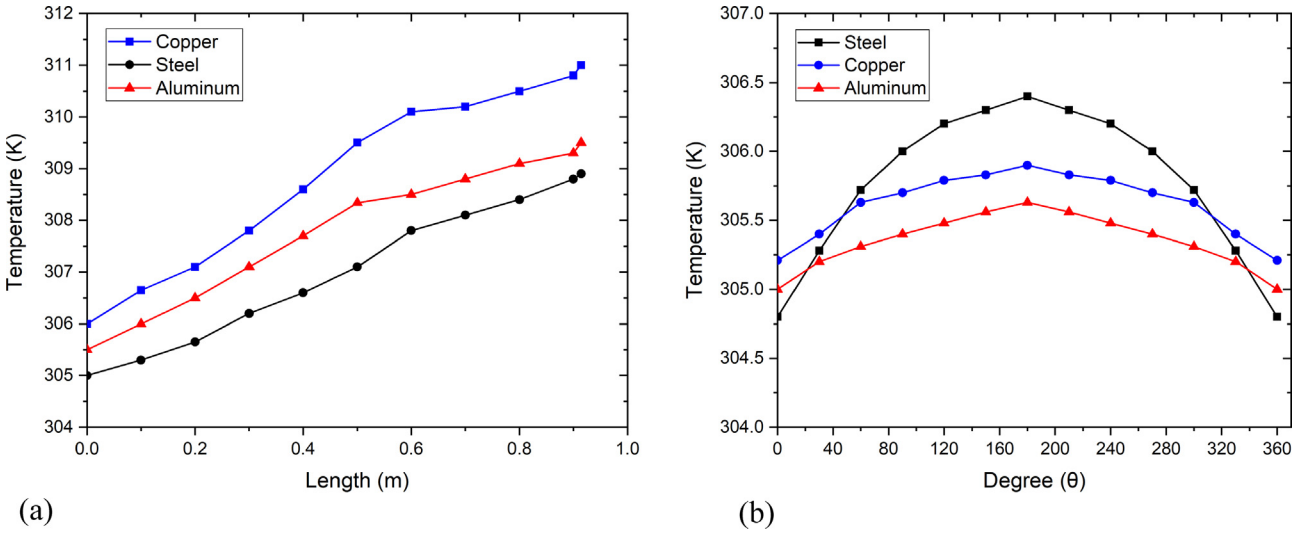

Fig. 4 Temperature distribution for different materials (a) along the length at top surce (b) along the circumference of the outlet at 0.0112 Kg/s mass flow rate and DNI 788 W/m$^{2.}$

nanofluids at a different mass flow rate, as demonstrated in the experiment. Simulated values show a slight increment than the experimental results. This is because the experiment might have slight experimental setups/measurement inaccuracies like in geometry modelling of collector, nanofluid synthesis, insulation of receiver tube, pumping disruption, etc., which cannot be evaded. It ultimately affects the behaviour of the experimental temperature values.

3. Results and discussion

The effect of absorber tube material on temperature distribution for steel, copper and aluminum absorber tube is investigated. The results obtained for different mass flow rates and their effect on the absorber tube temperature is analysed. Two nanofluids CuO in water and Alumina in water are used as working fluids.

3.1. Effect of absorber tube material on temprature distrubution

The Fig. 4 shows that the variation in the material change the distribution of the temperature of the tube of the absorber along the circumference. Due to better thermal conductivity, Copper tube shows a higher temperatures as compared to tubes made of Steel and Aluminum. The temperature throughout the circumference almost remains constant for copper and aluminum. However, the temperature increases for the first half of the circumference and then decreases at a regular pattern for steel made absorber tube.

The temperature contours obtained for of 302 K temperature is presented in Fig. 5. A lower outlet temperature was obtained using the steel tube outlets compared to tube made of copper and aluminum. The curved shape temperature distribution is due to low thermal conductivity of steel as compared to copper. The maximum temperature is achieved at the top surface, where there is the direct effect of heating on the circumference. The effect of radiations decreases along the circumference at the outlet of pipe and also compared [4]. It was observed that the difference between the inlet and outlet temperatures was low.

3.2. Comparison of mass flow rate for the temperature distribution

Fig. 6 shows the effect of different mass flow rates on the temperature distribution along the length of absorber tube made of aluminum using water as a working fluid. An increase in the mass flow rate from 0.0112 Kg/s to 0.0448 Kg/s decreases the surface temperature of the absorber tube due to a less interaction time is available between the fluid and absorber tube. The outlet temperature depends upon two factors: the convection heat transfer occurring between the fluid and tube, and

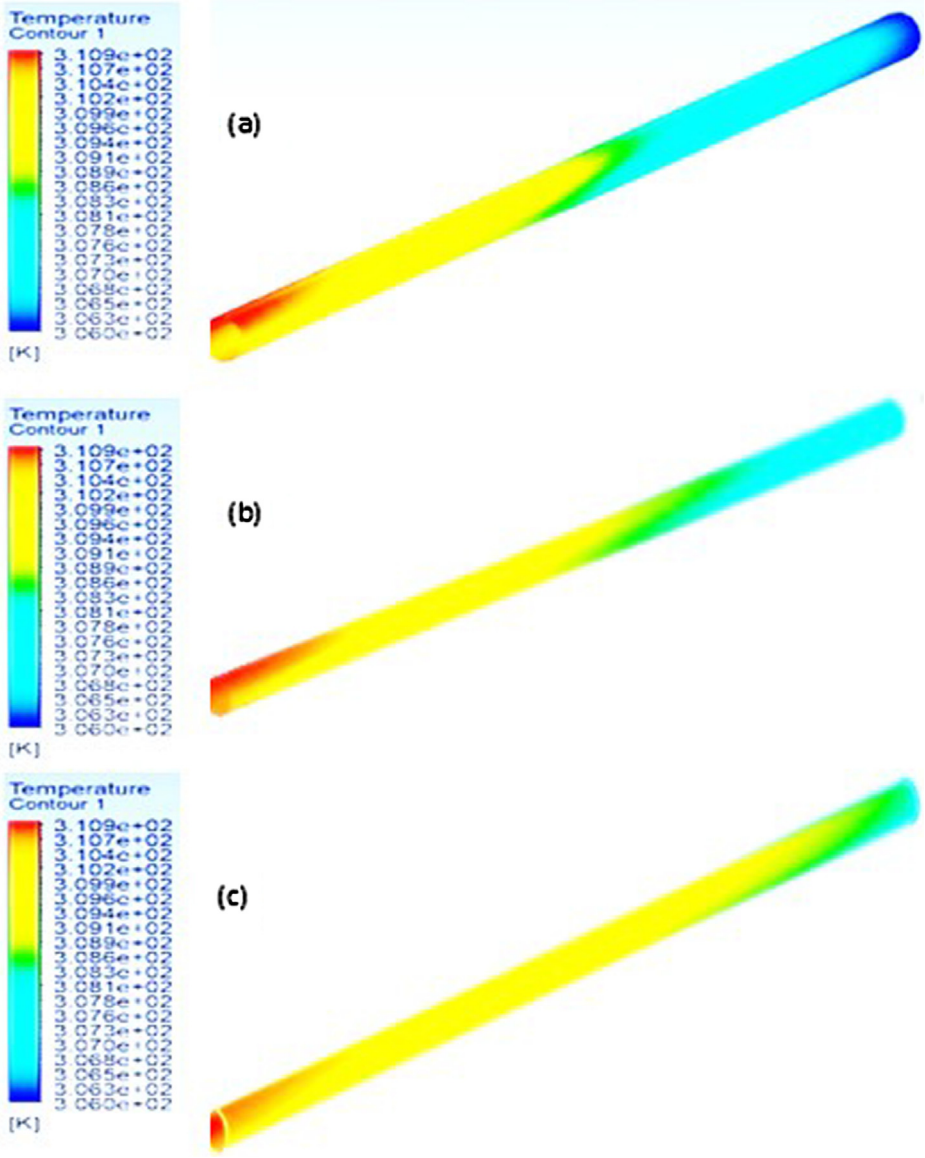

Fig. 5 Temperature Contours with absorber tube made of (a) copper (b) Aluminum (c) Stainless Steel using inlet temperature of 302 K and solar intensity of 773 W/m$^{2.}$

second is the velocity associated with mass flow rate. Moreover, it is also obvious that the temperature difference between inlet and outlet of tube is also reduced at higher flow rate of 0.0448 Kg/s as compared to 0.0112 Kg/s.

3.3. Comparison of thermal efficiency for aluminum Oxide-water

The experimental results of Sharma et al. [27] and simulated thermal efficiency of Al_2O_3-water at 0.0112 Kg/s and 0.0224 Kg/s with time is shown in Fig. 7. The thermal efficiency decreases with time due to lower solar intensity values; therefore, a low-temperature difference can be estimated between the inlet and outlet temperature at these time intervals. The maximum thermal efficiency for alumina nanofluid is observed from 9:30 to 10:30 AM, and then it starts to decrease till 3.00 PM. Since the thermal efficiency is not only depending on the solar irradiance, but also other parameters such as mass flow

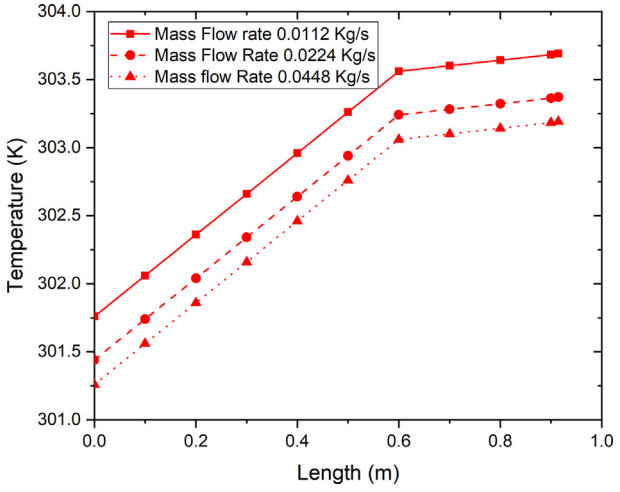

Fig. 6 Temperature along the length of absorber tube made of Aluminium at different flow rates.

rate, aperture diameter and specific heat of working fluid also affect the thermal performance of NPTSC. The experimental results from the literature were compared with the simulation data accordingly, which give level of accuracy in the experimental and simulation results. The overall thermal efficiency is 9.02% (simulated) and 8.65% (experimental) 0.0112 Kg/s mass flow rate as compared to 0.0224 Kg/s having overall efficiency of 8.34% (exp) and 8.39%. The low difference in thermal efficiency is due to low concentration of nano particles in the water i.e., 0.05 vol%. Increasing the vol.% of Alumina nano particles can result in increase in the thermal efficiency of the working fluid.

3.4. Comparison of thermal efficiency using CuO-water as a working fluid

The comparison in experimental and simulated thermal efficiency of CuO-water at 0.0112 Kg/s and 0.0224 Kg/s mass flow rate as shown in Fig. 8. There is no significant difference in the thermal efficiency using CuO-water by varying mass flow rates. The overall thermal efficiency is 9.03% (simulated) and 8.65% (experimental) for 0.01124 Kg/s as compared to 0.0224 Kg/s having overall efficiency of 8.9% (exp) and 9.62%.

3.5. Comparison of thermal efficiency using Al_2O_3 and CuO with different mass flow rates

The comparison of thermal efficiency of Alumina and CuO at a mass flow rate of 0.0112 Kg/s and 0.0224 Kg/s is shown in the Fig. 9. Both nanofluids show maximum efficiency w.r.t. time from 9:30 to 11:30 AM. The highest efficiency Al_2O_3 at a mass flow rate of 0.0112 Kg/s and 0.0224 L/hr. is 13.01 and 13.1%, respectively, while CuO has an efficiency of 13.92 and 14.79% at the same mass flow rates. Therefore, an approximately 1% increase in the thermal efficiency is observed in the case of CuO. Both nanofluids showed to faster

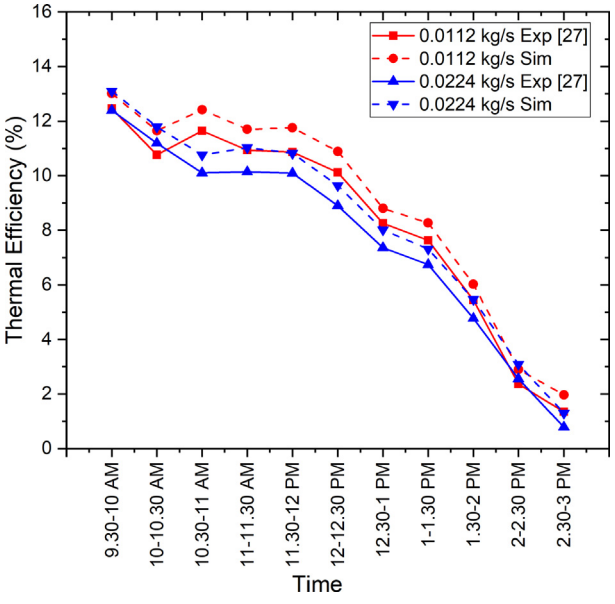

Fig. 7 Variation in Experimental and Simulated thermal efficiency of Al_2O_3-water atdifferent flow rates.

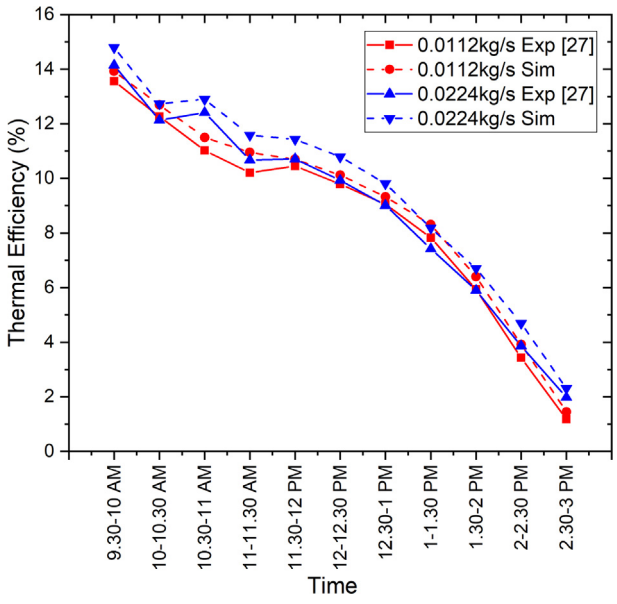

Fig. 8 Variation in Experimental and Simulated thermal efficiency of CuO-water at different flow rates.

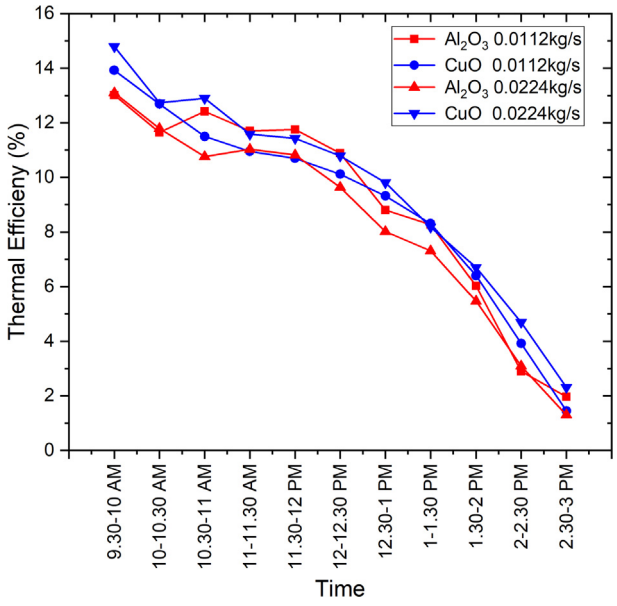

Fig. 9 Comparison of thermal efficiency usingAl_2O_3 and CuO at 0.0112 Kg/s and 0.0224 Kg/s mass flow rate.

variation in the temperature difference around 1 PM due to high radiation flux.

3.6. Comparison between variation of temperature of Al_2O_3 and CuO along length of tube

The comparison between the temperature variation for both Alumina-water and CuO-water is given in Fig. 10 and 11. It can be seen that CuO-water has higher outlet temperature as compared to Alumina for same inlet temperature. The CuO absorbs maximum solar radiation due to higher heat transfer coefficient and therefore, will result in higher thermal efficiency

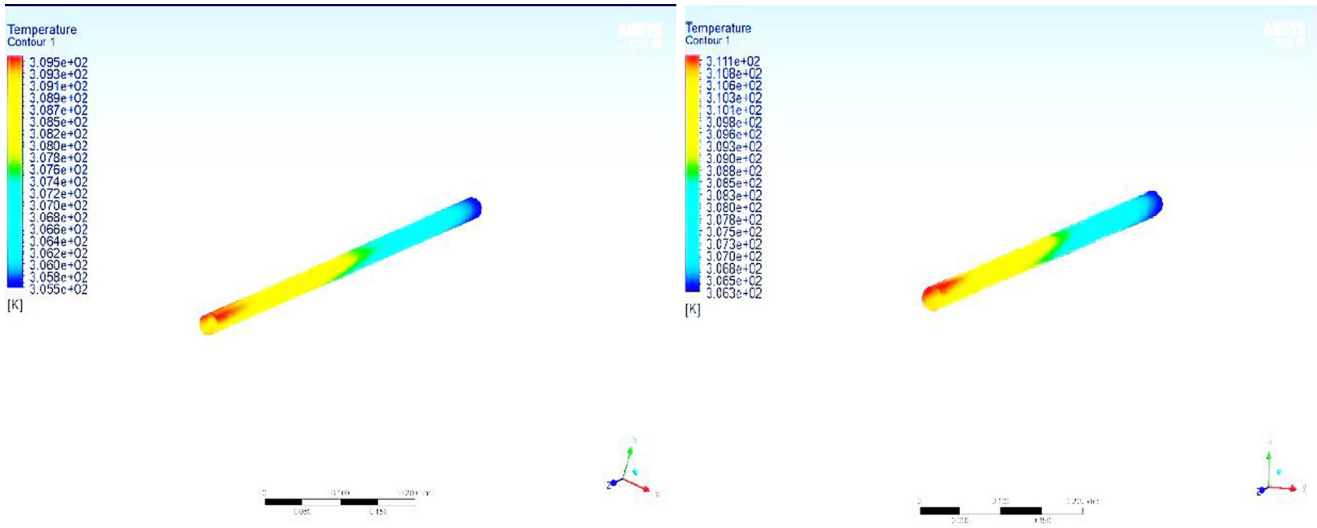

Fig. 10 Temperature Contour of Absorber tube (a)) for Aluminium Nanofluid (b) for Copper Nanofluid.

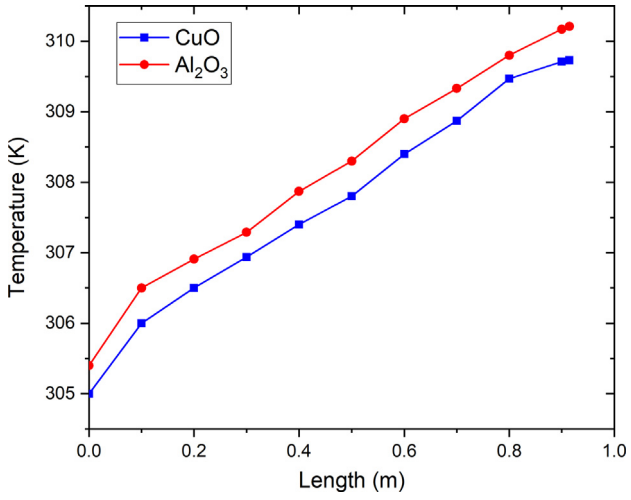

Fig. 11 Variation in temperatures for CuO-water and Alumina-Water nanofluid.

as compared to Alumina-water nanofluid. The inlet temperature of CuO is also higher than that of Al_2O_3 because of higher thermal conductivity of CuO as compared to Alumina nanofluid.

It can be seen from the above data that there is not much difference between the outlet temperatures of water and nanofluids. This is due to decreased length of the absorber tube as well as low volume concentration of nano particles in the water. Increasing the vol.% of nanoparticles in the water as well as increasing the length of the absorber tube can significantly affect the outlet temperature and thermal efficiency of PTSC [26,32]. The thermal efficiency is up to 1.2% by using Alumina nanofluid, while the thermal efficiency was 0.8% when CuO-Water nanofluid is used.

4. Conclusions

CFD simulations were carried out to study the effect of absorber tube material and nanofluids on thermal efficiency of NPTSC. The simulations demonstrate that the overall thermal performance can be increased up to 1–2% using nanofluids as the working fluid in PTSC. The CuO based nanofluids show higher outlet temperature as compared to Alumina based nanofluid at same heat flux and inlet temperature. An increase in mass flow rate of nanofluid also increases the thermal efficiency, a better thermal efficiency was observed using CuO based nanofluid at flow rate of 0.0224 Kg/s comparing with 0.0112 Kg/s. The material of absorber tube also affects the thermal efficiency of NTPC. Copper tube shows better thermal performance as compared to the Aluminum and stainless steel tubes. Density of a material allows the absorption of the solar radiations and thermal properties of the materials lead temperature distribution along the length of tube. Due to higher value of thermal conductivity, copper shows uniform temperature distribution along the length of the absorber tube. Further, the volume concentration of nanoparticles in nanofluids, size of NP, and composition of NP (hybrid nanoparticles (0-D), nanotubes/nanofibers (1-D), and highly conductive ionic liquids) as working fluid can also be investigated in NPTSC. Other parameters like the receiver tube's material's insulation and favourable geometry can also be studied via CFD and ANSYS analysis.

Declaration of Competing Interest

The authors declare that they have no known competing financial interests or personal relationships that could have appeared to influence the work reported in this paper.

Acknowledgments

The authors extend their appreciation to King Saud University for funding this work through Researchers supporting project number (RSP- 2021/133), King Saud University, Riyadh, Saudi Arabia.

References

[1] A. Shahsavari, M. Akbari, Potential of solar energy in developing countries for reducing energy-related emissions, Renew. Sustain. Energy Rev. 90 (March) (2018) 275–291, https://doi.org/10.1016/j.rser.2018.03.065.

[2] S.A. Hussnain, M. Farooq, M. Amjad, F. Riaz, Z.U.R. Tahir, M. Sultan, I. Hussain, M.A. Shakir, M.A. Qyyum, N. Han, A. Bokhari, Thermal Analysis and Energy Efficiency Improvements in Tunnel Kiln for Sustainable Environment, Processes 9 (9) (2021) 1629, https://doi.org/10.3390/pr9091629.

[3] Z.U. Rehman, M. Amjad, M. Asim, M. Azhar, M. Farooq, M.J. Ali, S.U. Ahmad, A. Hussain, Improving the accuracy of solar radiation estimation from reanalysis datasets using surface measurements, Sustain. Energy Technol. Assess. 47 (2021) 101485.

[4] Z. Alimohammadi, H.S. Akhijahani, Investigation of thermal Performance of a parabolic trough solar collector (PTSC) with different fluids using CFD method, pp. 11–12, 2019.

[5] J.A. Khan, M. Mustafa, T. Hayat, M. Turkyilmazoglu, A. Alsaedi, Numerical study of nanofluid flow and heat transfer over a rotating disk using Buongiorno's model, Int. J. Numer. Meth. Heat Fluid Flow 27 (1) (2017) 221–234.

[6] M. Turkyilmazoglu, On the transparent effects of Buongiorno nanofluid model on heat and mass transfer, Eur. Phys. J. Plus 136 (4) (2021) 1–15.

[7] M. Turkyilmazoglu, Performance of direct absorption solar collector with nanofluid mixture, Energy Convers. Manage. 114 (2016) 1–10.

[8] Z.u.R. Tahir, M. Asim, M. Azhar, G. Moeenuddin, M. Farooq, Correcting solar radiation from reanalysis and analysis datasets with systematic and seasonal variations, Case Stud. Therm. Eng. 25 (2021) 100933, https://doi.org/10.1016/j.csite.2021.100933.

[9] M. Khamooshi, H. Salati, F. Egelioglu, A. Hooshyar Faghiri, J. Tarabishi, S. Babadi, A review of solar photovoltaic concentrators, Int. J. Photoenergy 2014 (2014) 1–17, https://doi.org/10.1155/2014/958521.

[10] A. Sattar, M. Farooq, M. Amjad, M.A. Saeed, S. Nawaz, M.A. Mujtaba, S. Anwar, A.M. El-Sherbeeny, M.E.M. Soudagar, E. P. Bandarra Filho, Q. Ali, M. Imran, A. Pettinau, Performance Evaluation of a Direct Absorption Collector for Solar Thermal Energy Conversion, Energies 13 (18) (2020) 4956, https://doi.org/10.3390/en13184956.

[11] A. Siuta-Olcha, T. Cholewa, K. Dopieralska-Howoruszko, Experimental Investigations of Energy and Exergy Efficiencies of an Evacuated Tube Solar Collector, Proceedings 16 (1) (2019) 2, https://doi.org/10.3390/proceedings2019016002.

[12] A. Ghomrassi, H. Mhiri, P. Bournot, Numerical Study and Optimization of Parabolic Trough Solar Collector Receiver Tube, J. Sol. Energy Eng. Trans. ASME 137 (5) (2015), https://doi.org/10.1115/1.4030849.

[13] A. Gupta, W. Xuan, and R. Kumar, "Possible mechanisms for thermal conductivity enhancement in nanofluids," *Proc. 4th Int. Conf. Nanochannels, Microchannels Minichannels, ICNMM2006*, vol. 2006 B, pp. 987–995, 2006, doi: 10.1115/icnmm2006-96220.

[14] H.M. Şahin, E. Baysal, A.R. Dal, N. Şahin, Investigation of heat transfer enhancement in a new type heat exchanger using solar parabolic trough systems, Int. J. Hydrogen Energy 40 (44) (2015) 15254–15266, https://doi.org/10.1016/j.ijhydene.2015.03.009.

[15] S. Akbarzadeh, M.S. Valipour, Heat transfer enhancement in parabolic trough collectors: A comprehensive review, Renew. Sustain. Energy Rev. 92 (November 2017) (2018) 198–218, https://doi.org/10.1016/j.rser.2018.04.093.

[16] W. Fuqiang, L. Qingzhi, H. Huaizhi, T. Jianyu, Parabolic trough receiver with corrugated tube for improving heat transfer and thermal deformation characteristics, Appl. Energy 164 (2016) 411–424, https://doi.org/10.1016/j.apenergy.2015.11.084.

[17] Y. Wang, J. Xu, Q. Liu, Y. Chen, H. Liu, Performance analysis of a parabolic trough solar collector using Al2O3/synthetic oil nanofluid, Applied Thermal Engineering 107 (2016) 469–478.

[18] E. Bellos, C. Tzivanidis, Alternative designs of parabolic trough solar collectors, Prog. Energy Combust. Sci. 71 (2019) 81–117, https://doi.org/10.1016/j.pecs.2018.11.001.

[19] C. Ho, J. Christian, D. Gill, A. Moya, S. Jeter, S. Abdel-Khalik, D. Sadowski, N. Siegel, H. Al-Ansary, L. Amsbeck, B. Gobereit, R. Buck, Technology advancements for next generation falling particle receivers, Energy Procedia 49 (2014) 398–407, https://doi.org/10.1016/j.egypro.2014.03.043.

[20] R. Forristall, "Heat Transfer Analysis and Modeling of a Parabolic Trough Solar Receiver Implemented in Engineering Equation Solver," no. October, p. 164, 2003, doi: NREL/TP-550-34169.

[21] R. Loni, A.B. Kasaeian, O. Mahian, A.Z. Sahin, Thermodynamic analysis of an organic rankine cycle using a tubular solar cavity receiver, Energy Convers. Manag. 127 (2016) 494–503, https://doi.org/10.1016/j.enconman.2016.09.007.

[22] H. Liang, M. Fan, S. You, W. Zheng, H. Zhang, T. Ye, X. Zheng, A Monte Carlo method and finite volume method coupled optical simulation method for parabolic trough solar collectors, Appl. Energy 201 (2017) 60–68, https://doi.org/10.1016/j.apenergy.2017.05.047.

[23] M.A. Rehan, M. Ali, N.A. Sheikh, M.S. Khalil, G.Q. Chaudhary, T.u. Rashid, M. Shehryar, Experimental performance analysis of low concentration ratio solar parabolic trough collectors with nanofluids in winter conditions, Renew. Energy 118 (2018) 742–751, https://doi.org/10.1016/j.renene.2017.11.062.

[24] W. Fuqiang, C. Ziming, T. Jianyu, Y. Yuan, S. Yong, L. Linhua, Progress in concentrated solar power technology with parabolic trough collector system: A comprehensive review, Renew. Sustain. Energy Rev. 79 (February) (2017) 1314–1328, https://doi.org/10.1016/j.rser.2017.05.174.

[25] M. Zain, M. Amjad, M. Farooq, Z. Anwar, R. Shoukat, Enio P. Bandarra Filho, Du Xiaoze, Performance investigation of a solar thermal collector based on nanostructured energy materials, Front. Mater. 7 (2021) 462.

[26] E. Bellos, C. Tzivanidis, Investigation of a star flow insert in a parabolic trough solar collector, Appl. Energy 224 (March) (2018) 86–102, https://doi.org/10.1016/j.apenergy.2018.04.099.

[27] K. Sharma, L. Kundan, Nanofluid based concentrating parabolic solar collector (NBCPSC): A new alternative, Int. J. Res. Mech. Eng. Technol. 4 (2) (2014) 146–152.

[28] H. Khakrah, A. Shamloo, S. Kazemzadeh Hannani, Determination of Parabolic Trough Solar Collector Efficiency Using Nanofluid: A Comprehensive Numerical Study, J. Sol. Energy Eng. Trans. ASME 139 (5) (2017), https://doi.org/10.1115/1.4037092.

[29] D. Korres, E. Bellos, C. Tzivanidis, Investigation of a nanofluid-based compound parabolic trough solar collector under laminar flow conditions, Appl. Therm. Eng. 149 (2019) 366–376, https://doi.org/10.1016/j.applthermaleng.2018.12.077.

[30] I. Wole-osho, E.C. Okonkwo, S. Abbasoglu, D. Kavaz, Nanofluids in Solar Thermal Collectors: Review and Limitations, Int J Thermophys 41 (11) (2020), https://doi.org/10.1007/s10765-020-02737-1.

[31] G. Kumaresan, P. Sudhakar, R. Santosh, R. Velraj, Experimental and numerical studies of thermal performance enhancement in the receiver part of solar parabolic trough collectors, Renew. Sustain. Energy Rev. 77 (2017) 1363–1374, https://doi.org/10.1016/j.rser.2017.01.171.

[32] S. Kuharat and O. A. Bég, "Computational Fluid Dynamics Simulation of a Nanofluid-Based Annular Solar Collector with Different Metallic Nano-Particles," vol. 3, no. 1, 2019.

[33] E. Bellos, C. Tzivanidis, K.A. Antonopoulos, G. Gkinis, Thermal enhancement of solar parabolic trough collectors by using nano fl uids and converging-diverging absorber tube, Renew. Energy 94 (2016) 213–222, https://doi.org/10.1016/j.renene.2016.03.062.

[34] E. Bellos, C. Tzivanidis, Thermal analysis of parabolic trough collector operating with mono and hybrid nanofluids, Sustain. Energy Technol. Assess. 26 (2018) 105–115.

[35] A. Mwesigye, T. Bello-Ochende, J.P. Meyer, Heat transfer and entropy generation in a parabolic trough receiver with wall-detached twisted tape inserts, Int. J. Therm. Sci. 99 (2016) 238–257, https://doi.org/10.1016/j.ijthermalsci.2015.08.015.

[36] N.C. Roy, L.K. Saha, M. Sheikholeslami, Heat transfer of a hybrid nanofluid past a circular cylinder in the presence of thermal radiation and viscous dissipation, AIP Adv. 10 (9) (2020) 095208, https://doi.org/10.1063/5.0021258.

[37] H. Olia, M. Torabi, M. Bahiraei, M.H. Ahmadi, M. Goodarzi, M.R. Safaei, Application of Nanofluids in Thermal Performance Enhancement of Parabolic Trough Solar Collector: State-of-the-Art, Appl. Sci. 9 (3) (2019) 463, https://doi.org/10.3390/app9030463.

[38] M.V. Bozorg, M. Hossein Doranehgard, K. Hong, Q. Xiong, CFD study of heat transfer and fluid flow in a parabolic trough solar receiver with internal annular porous structure and synthetic oil–Al_2O_3 nanofluid, Renew. Energy 145 (2020) 2598–2614, https://doi.org/10.1016/j.renene.2019.08.042.

[39] M. Fan, H. Liang, S. You, H. Zhang, W. Zheng, J. Xia, Heat transfer analysis of a new volumetric based receiver for parabolic trough solar collector, Energy 142 (2018) 920–931, https://doi.org/10.1016/j.energy.2017.10.076.

[40] R.J. Braham, and A.T. Harris, ‘‘Review of Major Design and Scale-up Considerations for Solar Photocatalytic Reactors,” no. 8, pp. 8890–8905, 2009.

[41] İ.H. Yılmaz, A. Mwesigye, Modeling, simulation and performance analysis of parabolic trough solar collectors: A comprehensive review, Appl. Energy 225 (April) (2018) 135–174, https://doi.org/10.1016/j.apenergy.2018.05.014.

[42] S.A. Kalogirou, A detailed thermal model of a parabolic trough collector receiver, Energy 48 (1) (2012) 298–306, https://doi.org/10.1016/j.energy.2012.06.023.

[43] M. Pandey, B.N. Padhi, I. Mishra, Simulation and Modeling of Solar Trough Collector, Adv. Interdiscipl. Eng. Select Proc. FLAME 2019 (2018) 301–317, https://doi.org/10.1007/978-981-13-6577-5_29.

[44] E. Przenzak, M. Szubel, M. Filipowicz, The numerical model of the high temperature receiver for concentrated solar radiation, Energy Convers. Manag. 125 (2016) 97–106, https://doi.org/10.1016/j.enconman.2016.07.036.

[45] O. Behar, A. Khellaf, K. Mohammedi, A novel parabolic trough solar collector model - Validation with experimental data and comparison to Engineering Equation Solver (EES), Energy Convers. Manag. 106 (2015) 268–281, https://doi.org/10.1016/j.enconman.2015.09.045.

[46] E. Esmaeilzadeh, H. Almohammadi, S. Nasiri Vatan, A.N. Omrani, Experimental investigation of hydrodynamics and heat transfer characteristics of γ-Al 2O 3/water under laminar flow inside a horizontal tube, Int. J. Therm. Sci. 63 (2013) 31–37, https://doi.org/10.1016/j.ijthermalsci.2012.07.001.

[47] M. Sardarabadi, M. Passandideh-Fard, S. Zeinali Heris, Experimental investigation of the effects of silica/water nanofluid onPV/T (photovoltaic thermal units), Energy 66 (2014) 264–272, https://doi.org/10.1016/j.energy.2014.01.102.

[48] İ.H. Yılmaz, A. Mwesigye, Modeling, simulation and performance analysis of parabolic trough solar collectors: A comprehensive review, Appl. Energy 225 (May) (2018) 135–174, https://doi.org/10.1016/j.apenergy.2018.05.014.

[49] K. G. Kandwal, S. Lal, ‘‘An Experimental Investigation into the Performance of a Nanofluid Based Concentrating Parabolic Solar Collector (NCPSC),” no. July, 2014.

[50] B. Chico, I. Díaz, J. Simancas, M. Morcillo, Annual Atmospheric Corrosion of Carbon Steel Worldwide. An Integration of ISOCORRAG, ICP/UNECE and MICAT Databases, Materials (Basel) 10 (6) (2017) 601, https://doi.org/10.3390/ma10060601.

[51] M. Akrami, H. Alsari, A.A. Javadi, M. Dibaj, R. Farmani, H.E. S. Fath, A.H. Salah, A. Negm, Analysing the material suitability and concentration ratio of a solar-powered parabolic trough collector (PTC) using computational fluid dynamics, Energies 13 (20) (2020) 5479, https://doi.org/10.3390/en13205479.

[52] Z. Ahmed, Atmospheric Corrosion, Princ. Corros. Eng. Corros Control (2006) 550–575, https://doi.org/10.1201/9781420067712-8.

[53] Y.A. Cengel, M.A. Boles, M. Kanoglu, Thermodynamics: an engineering approach, McGraw-hill, New York, 2011.